RESEARCH ARTICLE SUMMARY

PLANETARY SCIENCE

The geomorphology of Ceres

D. L. Buczkowski,* B. E. Schmidt, D. A. Williams, S. C. Mest, J. E. C. Scully, A. I. Ermakov, F. Preusker, P. Schenk, K. A. Otto, H. Hiesinger, D. O'Brien, S. Marchi, H. Sizemore, K. Hughson, H. Chilton, M. Bland, S. Byrne, N. Schorghofer, T. Platz, R. Jaumann, T. Roatsch, M. V. Sykes, A. Nathues, M. C. De Sanctis, C. A. Raymond, C. T. Russell

INTRODUCTION: Observations of Ceres, the largest object in the asteroid belt, have suggested that the dwarf planet is a geologically differentiated body with a silicate core and an ice-rich mantle. Data acquired by the Dawn spacecraft were used to perform a three-dimensional characterization of the surface to determine if the geomorphology of Ceres is consistent with the models of an icy interior.

RATIONALE: Instruments on Dawn have collected data at a variety of resolutions, including both clear-filter and color images. Digital terrain models have been derived from stereo images. A preliminary 1:10 M scale geologic map of Ceres was constructed using images obtained during the Approach and Survey orbital phases of the mission. We used the map, along with higher-resolution imagery, to assess the geology of Ceres at the global scale, to identify geomorphic and structural features, and to determine the geologic processes that have affected Ceres globally.

RESULTS: Impact craters are the most prevalent geomorphic feature on Ceres, and several of the craters have fractured floors. Geomorphic analysis of the fracture patterns shows that they are similar to lunar Floor-Fractured Craters (FFCs), and an analysis of the depth-to-diameter ratios shows that they are anomalously shallow compared with average Ceres craters. Both of these factors are consistent with FFC floors being uplifted due to an intrusion of cryomagma.

Kilometer-scale linear structures cross much of Ceres. Some of these structures are oriented radially to large craters and most likely formed due to impact processes. However, a set of linear structures present only on a topographically high region do not have any obvious relationship to impact craters. Geomorphic analysis suggests that they represent subsurface faults and might have formed due to crustal uplift by cryomagmatic intrusion.

ON OUR WEBSITE

Read the full article at http://dx.doi.org/10.1126/science.aaf4332

Domes identified across the Ceres surface present a wide range of sizes (<10 km to >100 km), basal shapes, and profiles. Whether a single formation mechanism is responsible for their formation is still an open question. Cryovolcanic extrusion is one plausible process for the larger domes, although most small mounds (<10-km diameter) are more likely to be impact debris.

Differences in lobate flow morphology suggest that multiple emplacement processes have operated on Ceres, where three types of flows have been identified. Type 1 flows are morphologically similar to ice-cored flows on Earth and Mars. Type 2 flows are comparable to long-runout landslides. Type 3 flows morphologically resemble the fluidized ejecta blankets of rampart craters, which are hypothesized to form by impact into ice-rich ground.

CONCLUSION: The global trend of lobate flows suggests that differences in their geomorphology could be explained by variations in ice content and temperature at the near surface. Geomorphic and topographic analyses of the FFCs suggest that cryomagmatism is active on Ceres, whereas the large domes are possibly formed by extrusions of cryolava. Although spectroscopic analysis to date has identified water ice in only one location on Ceres, the identification of these potentially ice-related features suggests that there may be more ice within localized regions of Ceres' crust. ■

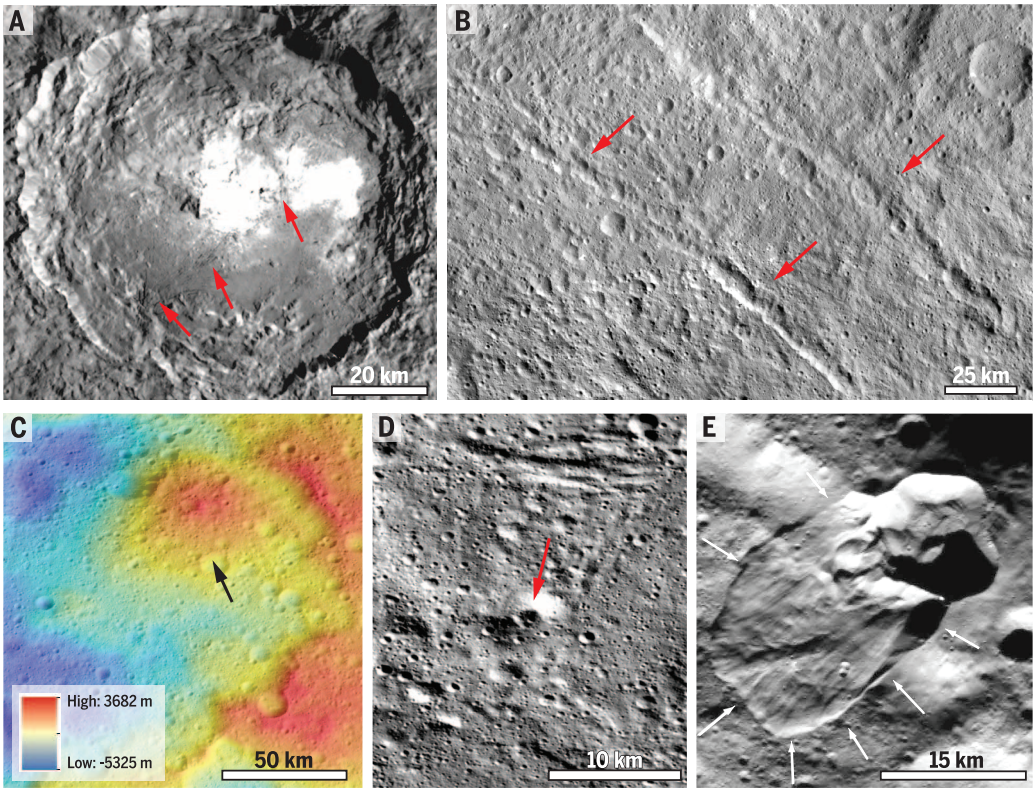

Dawn High-Altitude Mapping Orbit imagery (140 m per pixel) of example morphologic features. (**A**) Occator crater; arrows point to floor fractures. (**B**) Linear structures, denoted by arrows. (**C**) A large dome at 42° N, 10° E, visible in the elevation map. (**D**) A small mound at 45.5° S, 295.7° E. (**E**) Type 1 lobate flow; arrows point to the flow front.

The list of author affiliations is available in the full article online.
*Corresponding author. Email: debra.buczkowski@jhuapl.edu
Cite this article as D. L. Buczkowski *et al.*, *Science* 353, aaf4332 (2016). DOI: 10.1126/science.aaf4332

RESEARCH ARTICLE

PLANETARY SCIENCE

The geomorphology of Ceres

D. L. Buczkowski,[1*] B. E. Schmidt,[2] D. A. Williams,[3] S. C. Mest,[4] J. E. C. Scully,[5] A. I. Ermakov,[6] F. Preusker,[7] P. Schenk,[8] K. A. Otto,[7] H. Hiesinger,[9] D. O'Brien,[4] S. Marchi,[10] H. Sizemore,[4] K. Hughson,[11] H. Chilton,[2] M. Bland,[12] S. Byrne,[13] N. Schorghofer,[14] T. Platz,[15] R. Jaumann,[7] T. Roatsch,[7] M. V. Sykes,[4] A. Nathues,[15] M. C. De Sanctis,[16] C. A. Raymond,[5] C. T. Russell[11]

Analysis of Dawn spacecraft Framing Camera image data allows evaluation of the topography and geomorphology of features on the surface of Ceres. The dwarf planet is dominated by numerous craters, but other features are also common. Linear structures include both those associated with impact craters and those that do not appear to have any correlation to an impact event. Abundant lobate flows are identified, and numerous domical features are found at a range of scales. Features suggestive of near-surface ice, cryomagmatism, and cryovolcanism have been identified. Although spectroscopic analysis has currently detected surface water ice at only one location on Ceres, the identification of these potentially ice-related features suggests that there may be at least some ice in localized regions in the crust.

The Dawn spacecraft (*1*) left Vesta in late 2012 and went into orbit around Ceres on 6 March 2015. Framing Camera (*2*) images were taken during the Approach (1.3 km/pixel), Survey (415 m/pixel), High-Altitude Mapping Orbit (HAMO) (140 m/pixel), and Low-Altitude Mapping Orbit (LAMO) (35 m/pixel) phases of the mission (*3*). Clear filter and color images, together with digital terrain models derived from stereo images, have enabled a three-dimensional characterization of the surface, which we have used to determine whether the geomorphology of Ceres is consistent with models of the dwarf planet having an icy interior (*3*).

Geologic mapping

As was done at Vesta (*4*), a geological mapping campaign was conducted at Ceres. A preliminary geologic map at a scale of 1:10 M was constructed using images obtained during the Approach and Survey orbital phases (Fig. 1). Surface features have been organized into discrete map units that are defined and characterized based on physical attributes such as albedo, morphology, structure, color, and topography. These units were then related to the putative geologic processes that produced them, such as volcanism, tectonism, impact cratering, and/or deposition.

Stereophotogrammetric analysis of Ceres was used in the geologic mapping, and it showed that there is ~15 km of relief (Fig. 2A), referenced to the mean radius, considerably less than the ~41 km of total relief that was observed on Vesta (*5*). Although analysis of the topography suggested that there is no obvious elevation that discriminates between highlands and lowlands, one discrete topographically high region centered at 15°N, 230°E (*3*) was identified and named Hanami Planum (Fig. 2A, white dashed circle).

We used the map to assess the geology of Ceres at the global scale, to identify geomorphic and structural features, and to determine the geologic processes that have affected Ceres globally. Geomorphic features identified on Ceres include impact craters, linear structures, domical features, and lobate flows.

Impact craters

Impact craters are the most prevalent geomorphic feature on Ceres (*6*), and resurfacing appears to be primarily driven by impact (*6*). Regions of low crater density are strongly associated with major craters, such as Urvara, Yalode, and Kerwan (*6*) (Fig. 1). Before Dawn's arrival, it was expected that most craters on Ceres would be relaxed (*7*), but instead there is a large inventory of craters with sharp walls and deep floors (*6*).

To study the dynamic range of the topography of Ceres, we created a hypsogram, which displays the elevation of Ceres plotted against the percentage of surface area at that elevation (Fig. 2). Previously published hypsograms for the rocky planets (Mercury, Venus, Earth, and Mars) have a positive skew because mountainous terrain and in-filled depressions lead to a long tail of positive topography (Fig. 2C). However, the hypsogram of Ceres topography shows a unimodal distribution that skews slightly (–0.17) toward the negative (Fig. 2B). This is similar to the hypsogram for the icy moon Titan, which is also slightly negatively skewed. On Titan, this negative skew was determined to represent a significant population of unfilled depressions (*8*). It is likely that the unexpectedly large inventory of nonrelaxed craters on Ceres similarly skews its hypsogram toward a slightly longer tail of negative topography (Fig. 2B).

Occator crater

A number of small anomalously bright features were observed during the Approach to Ceres. The brightest of these occur in the center and northeastern floor of Occator, a 92-km-diameter crater centered at 19.9°N, 239.1°E, (Fig. 3). The Occator bright spots coincide with one of two longitudes where observations by the Herschel space telescope suggested water vapor emission from Ceres (*9*).

Occator's crater rim is scalloped, with multiple straight segments and several 90° bends, and its walls are terraced (Fig. 3A). The crater has ~4 km of relief from floor to rim (Fig. 3B). A smooth to knobby floor material embays the terraced wall material but is overlain by lobate flows whose margins suggest that they emanate from the center of the crater (Fig. 3C). Many of the bright-spot materials in Occator overlie the lobate flows and are strongly associated with fractures on its floor (Fig. 3, A to C). However, the largest bright spot is associated with a 9-km-wide, ~1-km-deep central pit (*6*, *10*) that has a 2-km-wide, ~400-m-high central dome on its floor (*6*). Similar domes have been identified in large (>60-km diameter) central pit craters on Ganymede and Callisto (*11*); it has been hypothesized that these domes form due either to uplift of the surface during the impact event or to postimpact cryomagmatic intrusions in craters that impacted where target materials were ice-rich (*11*, *12*). The similarity of the morphology of the Occator pit and dome to those seen in impact craters on Ganymede and Callisto implies that similar mechanisms may be operating on these three bodies. Therefore, the association of the most prominent bright spot in Occator with the central structure suggests that either uplift or localized extrusion is involved in bright-spot formation.

Floor-Fractured Craters

Several of the impact craters on Ceres have patterns of fractures on their floors (Figs. 3D and 4). These fractures appear similar to those found within a class of lunar craters referred to as Floor-Fractured Craters (FFCs) (*13*). Lunar FFCs are characterized by crater floors cut by radial, concentric, and/or polygonal fractures (*13*). The depth versus diameter (*d*/*D*) relationship of the FFCs is distinctly shallower than the same association for other lunar craters (*14*). FFCs have been classified into crater classes, Types 1 to 6, based on their morphometric properties (*13*–*15*). Models for FFC formation have invoked both floor uplift due to magmatic intrusion beneath the crater (*13*–*15*) or floor shallowing due to

[1]Johns Hopkins University Applied Physics Laboratory, Laurel, MD 20723, USA. [2]Georgia Institute of Technology, Atlanta, GA 30332, USA. [3]Arizona State University, Tempe, AZ 85287, USA. [4]Planetary Science Institute, Tucson, AZ 85719, USA. [5]NASA Jet Propulsion Laboratory, La Cañada Flintridge, CA 91011, USA. [6]Massachusetts Institute of Technology, Cambridge, MA 02139, USA. [7]German Aerospace Center (DLR), Berlin 12489, Germany. [8]Lunar and Planetary Institute, Houston, TX 77058, USA. [9]Westfälische Wilhelms-Universität Münster, Münster 48149, Germany. [10]Southwest Research Institute, Boulder, CO 80302, USA. [11]University of California, Los Angeles, CA 90095, USA. [12]United States Geological Survey, Flagstaff, AZ 86001, USA. [13]Lunar and Planetary Laboratory, Tucson, AZ 85721, USA. [14]University of Hawaii at Manoa, Honolulu, HI 96822, USA. [15]Max Planck Institute for Solar System Research, Göttingen 37077, Germany. [16]Istituto di Astrofisica e Planetologia Spaziale INAF, Rome 00133, Italy.
*Corresponding author. Email: debra.buczkowski@jhuapl.edu

viscous relaxation [e.g., (*16*)] to explain their anomalously shallow floors.

FFCs have also been identified on Mars (*17*). Martian FFCs exhibit morphological characteristics similar to the lunar FFCs, but many of their rims have been highly dissected. Analyses suggest that the martian FFCs also formed due to volcanic activity but that the final morphologies were heavily influenced by interactions with groundwater and/or ice (*17*).

As on the Moon, the style of fracturing within Ceres FFCs can vary from crater to crater. We have cataloged the Ceres FFCs according to the classification scheme designed by (*13*) and used by (*14*, *15*). Occator crater has several sets of fractures on its floor, including circumferential fractures encircling the central pit, linear fractures crossing its floor, and circumferential fractures close to the crater wall (Fig. 3D). Dantu crater (126-km diameter) similarly has both circumferential and radial fractures on its floor (Fig. 4A), whereas Azacca crater (49.9-km diameter) has only linear fractures (Fig. 4B). These large (>50 km) craters are most consistent with Type 1 lunar FFCs, which are described as generally large craters with deep floors, central peak complexes, extensive wall terraces, and radial and/or concentric fractures (*13*); they were found to be most consistent with formation by magmatic intrusion (*15*, *16*).

Other craters on Ceres are more consistent with Type 4 FFCs (*13*). These lunar craters are defined by the presence of a V-shaped moat separating the wall scarp from the crater interior. However, there are three subclasses (4a, 4b, and 4c) that differ in the depth of the moat, whether there is an inner ridge associated with the moat, and how pronounced the floor fractures are (*15*). Viscous relaxation models were unable to produce moats of any shape in the crater interiors (e.g., *16*, *18*), but in magmatic intrusion models, a V-shaped moat marks the extent of the subsurface intrusion (*15*). Lociyo crater is representative of a Ceres Type 4b crater. It has a hummocky interior, with subdued grooves instead of sharp fractures (Fig. 4C), and its topographic profile shows V-shaped moats and interior ridges (Fig. 4E).

An analysis of the *d*/*D* ratio of the Ceres FFCs shows that they are anomalously shallow compared with average Ceres craters (Fig. 4D). The shallow *d*/*D* of Ceres FFCs is similar to that observed for the lunar FFCs (*15*) and suggests that these craters may also be experiencing an intrusion of a low-density material from below the craters that has uplifted their floors. Although on the Moon and Mars the intrusive material is hypothesized to be silicate magma, this is unlikely for Ceres. However, a cryovolcanic extrusive edifice has been identified on Ceres (*19*), suggesting that cryomagmatic intrusions could be responsible for the formation of the Ceres FFCs.

Polygonal craters

Polygonal craters, a type of crater whose rims are composed of at least two straight segments, are widespread on Ceres (Fig. 5). These angular craters are commonly found on asteroids, such as Mathilde (*20*), Eros (*21*), and Lutetia (*22*), and have also been identified on icy moons such as Iapetus (*23*) and Dione (*24*). Polygonal craters have been hypothesized to form when preexisting subsurface fracturing affects crater formation (*20*), causing crater rims to form parallel to preexisting planes of weakness (*25*, *26*). Their widespread presence on Ceres suggests that the

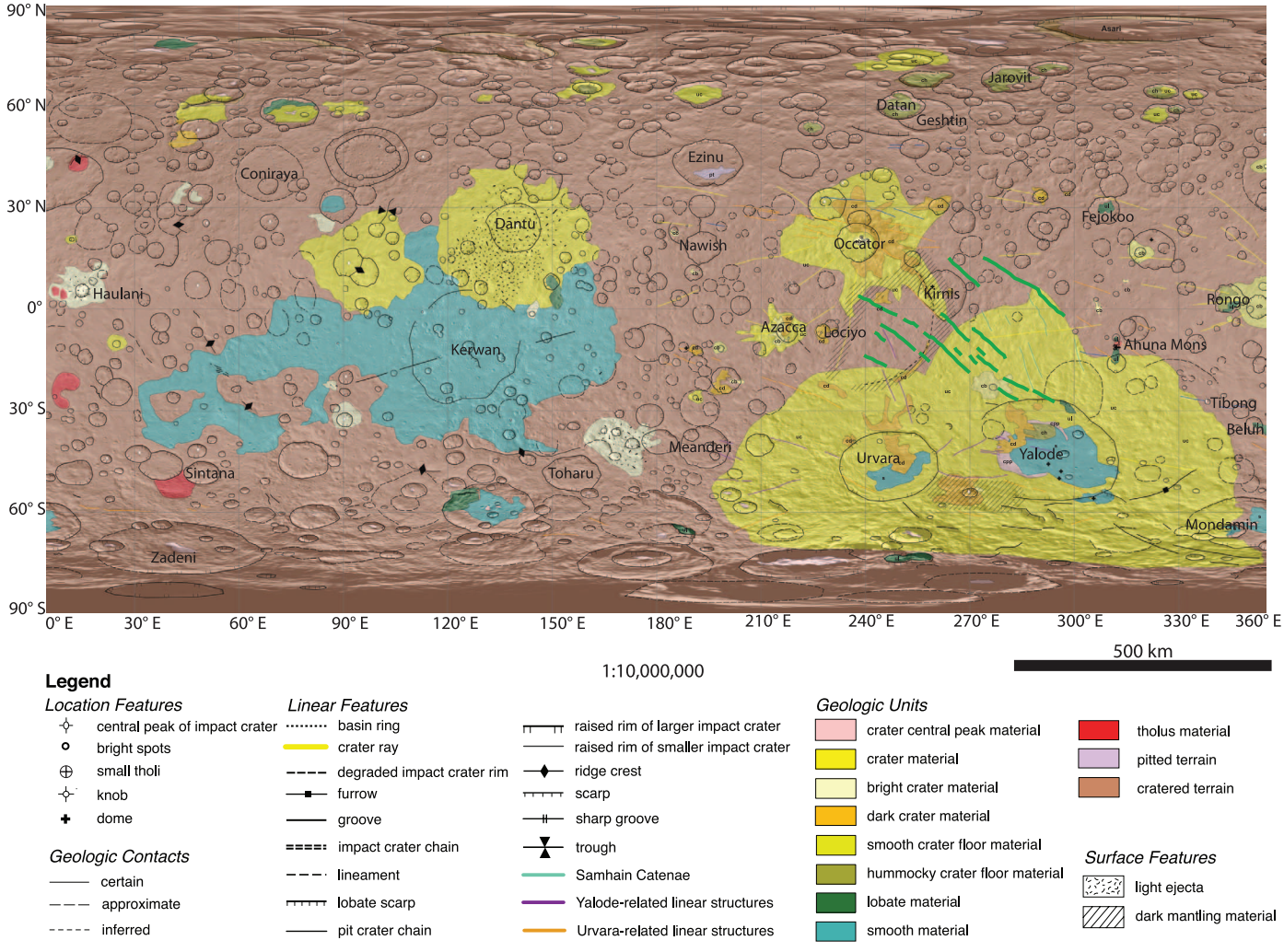

Fig. 1. The geologic map of Ceres based on Survey orbit data. The map, presented at 1:10 M scale, is displayed in simple cylindrical projection, with legend.

crust is extensively fractured, which in turn suggests that the near-surface crust must be both brittle enough to fracture and strong enough to retain fractures for long periods of time (*3*).

Linear structures

Kilometer-scale linear structures—including grooves, pit crater chains, fractures, and troughs—cross much of Ceres (Figs. 1 and 6). Some of these structures appear to be radial to the large craters Urvara and Yalode (Fig. 6A) and most likely formed due to impact processes. However, a set of regional linear structures named the Samhain Catenae do not have any obvious relationship to impact craters, and a geomorphic analysis suggests that they represent subsurface faults.

The majority of the Samhain Catenae are made up of linear assemblages of small depressions, although there are also some grooves and one large trough identified as belonging to this group of structures. The lack of raised rims on the merged pits of the Samhain Catenae (Fig. 6B) makes it unlikely that these are secondary crater chains (*27*). Instead, the morphology of the Samhain Catenae more closely resembles that of pit crater chains, a type of feature identified on many planetary bodies, including Earth, Mars, Enceladus, Eros, and Vesta (*28*). There is a strong correlation between pit crater chains and fault-bounded graben on Mars (*29*), and they have been hypothesized to represent buried normal faults on a number of small bodies (*28*). The theory suggests that sudden widening (dilation) at steep sections

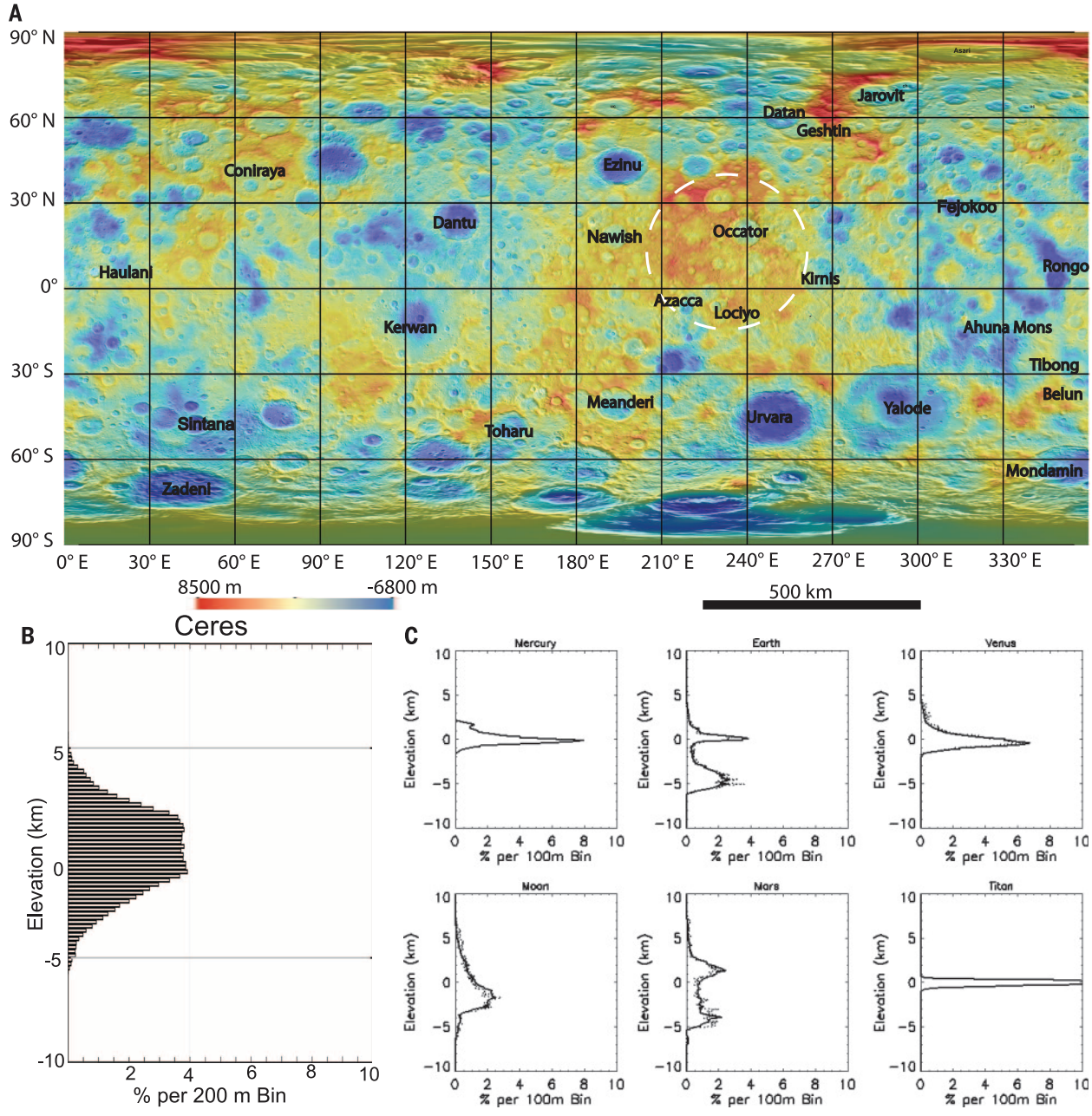

Fig. 2. Ceres topography. (**A**) Stereophotogrammetric digital terrain model of Ceres (displayed in simple cylindrical projection), overlying the Survey global mosaic. Heights are relative to the triaxial ellipsoid dimensions (482 by 482 by 446 km). The white dashed circle outlines Hanami Planum. (**B**) The Ceres hypsogram, which shows elevations as height above the equipotential surface of Ceres as determined by the gravity field (CERES 18b, truncated at degree 11). The standard deviation is 1.842 km, the skewness is −0.17, and the kurtosis is 2.65. The curve has a slightly longer tail in the negative direction. (**C**) Hypsograms of Mercury, Venus, Earth, Mars, the Moon, and Titan from (*8*), for comparison. Only Earth and Mars have bimodal distributions. Most hypsograms have a positive skew, with a long tail in the positive direction. Only Titan shows a negative skew, similar to that found for Ceres.

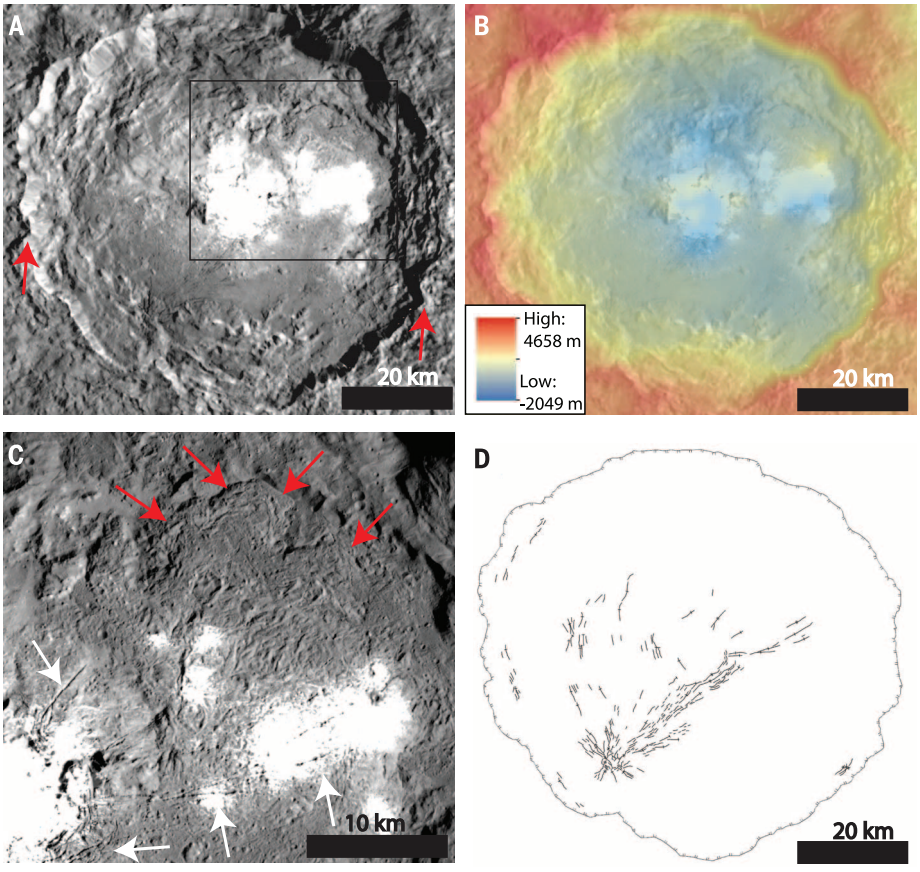

Fig. 3. Occator crater. (**A**) HAMO mosaic of Occator crater (140 m/pixel). North is up. Inset shows location of (C). Red arrows point to 90° bends in the crater rim. (**B**) HAMO topography of Occator overlain on the HAMO mosaic. (**C**) LAMO resolution (35 m/pixel) mosaic of the lobate flows in Occator. Red arrows point to flow margins. White arrows point to fractures on the crater floor. (**D**) Map of the fractures on the floor of Occator. The crater rim is outlined.

of the buried fault causes overlying material to collapse into the openings along its length (*29*). The individual pits can then merge together to form merged pits, and eventually grooves, as the feature matures (*29*). This maturation of pit crater chains is a probable cause for the occasional groove and merged pits found among the Samhain Catenae (Fig. 6B).

Polygonal craters in close proximity to the Samhain Catenae have straight crater rims aligned with the grooves and troughs (Fig. 5). This alignment supports our inference that the Samhain Catenae are in fact fracture systems, not ejecta scour or secondary craters. The orientation of the Samhain Catenae relative to each other is suggestive of en echelon fractures; many of the longer Samhain Catenae are made up of smaller structures that have joined together via S-shaped linkages (Fig. 6B). A cross section of one Samhain Catena structure is displayed in the wall of Occator crater, at the locations where the crater rim suddenly bends 90° in both the western and eastern walls of the crater (Figs. 3A and 6C). Profile views of the Occator wall at these locations suggest that (i) the structure dips ~60° and (ii) there is downward motion on the hanging wall, strongly implying normal faulting. Many of the Samhain Catenae are crosscut by the linear features radial to Urvara and Yalode (Fig. 6A), indicating that they are older than fractures formed during those impact events.

By mapping the Samhain Catenae directly onto the Ceres shape model and modeling them as planes that cut through the dwarf planet, we were able to determine an approximate strike and dip for the underlying faults by plotting the pole directions of the modeled planes on a lower-hemisphere graph (a stereonet) (Fig. 6D). Clustering of the pole directions (Fig. 6D) suggests that the

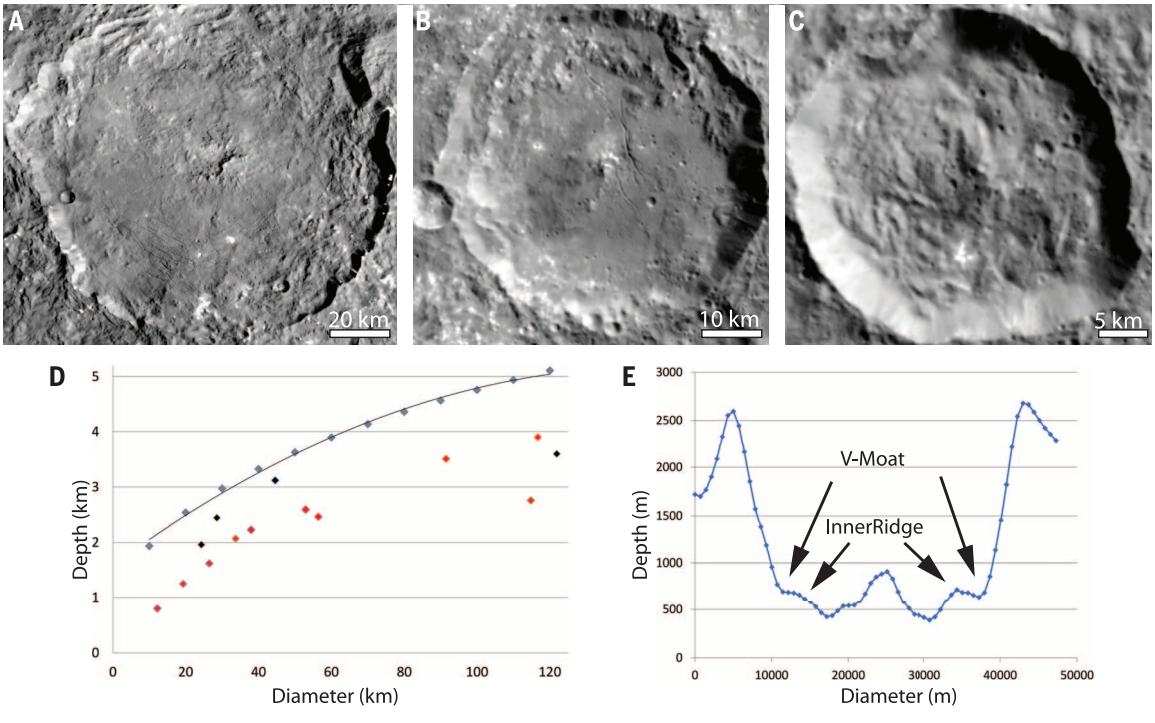

Fig. 4. FFCs. HAMO mosaics (140 m/pixel) of (**A**) Dantu crater, (**B**) Azacca crater, and (**C**) Lociyo crater. (**D**) Depth-to-diameter ratio of the FFCs currently identified on Ceres. Red dots are FFCs on Hanami Planum; black dots represent FFCs located elsewhere on Ceres. The black line is a second-order polynomial fit to the depth-to-diameter ratio for the average Ceres crater, as derived by (*6*). (**E**) The topographic profile of Lociyo crater shows the V-shaped moats and interior ridges characteristic of a Type 4 FFC.

Samhain Catenae represent similarly oriented planes and implies a common formation mechanism of the corresponding structures. In similar analyses of linear structures on Vesta (*5*) and Eros (*30*), the coordinates of the pole cluster correlated to an impact crater, which was then theorized to have produced the impact stresses that caused the faults to form. However, the poles of the Samhain Catenae do not correspond to any visible impact crater on Ceres, making it unlikely that they formed due to impact stresses.

The extent of the Samhain Catenae is constrained to Hanami Planum (Figs. 1 and 2). This roughly circular, topographically high region, 555 km in diameter, is also the location of many of the currently identified FFCs (Fig. 4, red dots). If we accept that the FFCs have fractured floors due to cryomagmatic intrusion beneath their floors, as is thought for the Moon (*13*–*15*), then it seems reasonable to hypothesize that the high-standing regions that they are predominantly found upon may be elevated due to intrusion of a lower-density material. The uplift of the crust due to this putative intrusion could possibly be responsible for the formation of the Samhain Catenae.

Patterns of smaller-scale linear structures have been identified on the topographic high regions

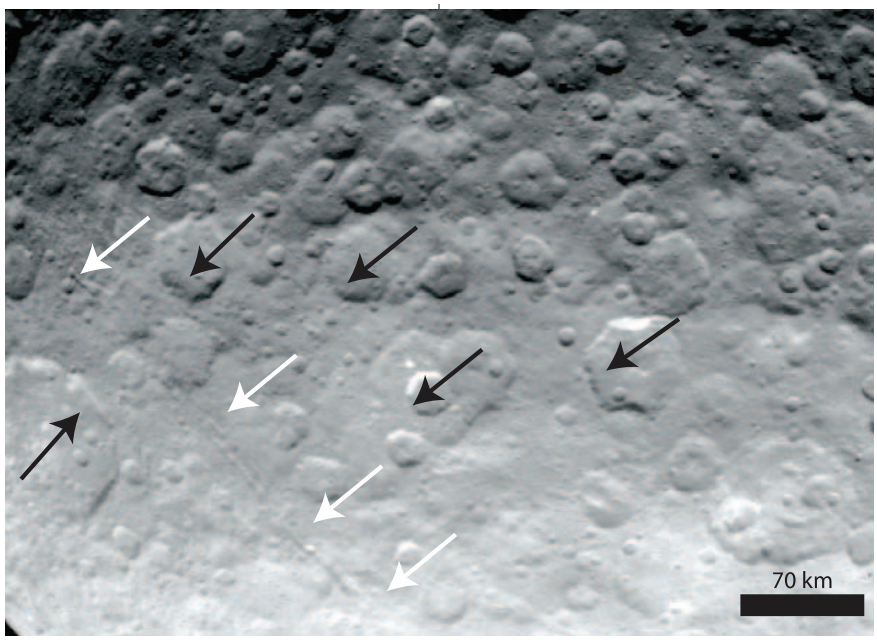

Fig. 5. Polygonal craters. A Survey (415 m/pixel) image of Ceres showing several polygonal craters in the vicinity of kilometer-scale linear structures (white arrows). Black arrows point to the straight rims of polygonal craters that are aligned with the Samhain Catenae.

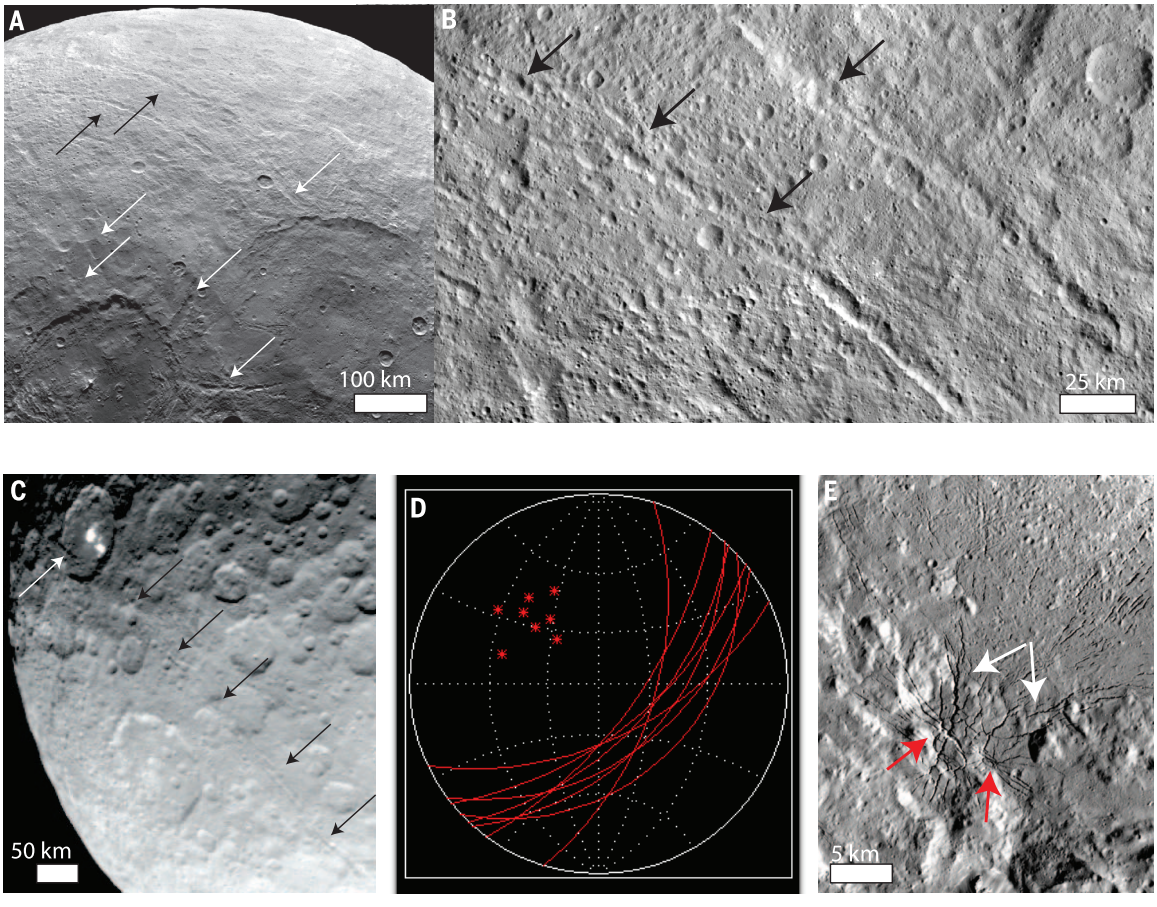

Fig. 6. Regional linear structures. (**A**) Survey image (415 m/pixel) of Urvara (left) and Yalode (right) craters. White arrows point to linear structures radial to the craters. Black arrows point to linear structures in (B). (**B**) HAMO (140 m/pixel) Framing Camera clear-filter image of regional linear structures (north is up). The pits do not have rims, suggesting that these are pit crater chains (PCCs), not impact crater chains. The northernmost PCC deforms the southwestern rim of Kirnis crater. Black arrows point to S-shaped junctions connecting three smaller en echelon structures. (**C**) Survey image (415 m/pixel) of a regional linear structure (black arrows) that cuts the rim of Occator crater (white arrow points to 90° bend in Occator's western rim). (**D**) Stereonet plots of the Samhain Catenae. Pole positions cluster, centered at ~45°N, ~300°E. (**E**) LAMO image (35 m/pixel) of a system of fractures at 16.6°N, 237.1°E that strongly resembles fracturing associated with asymmetric domal uplift.

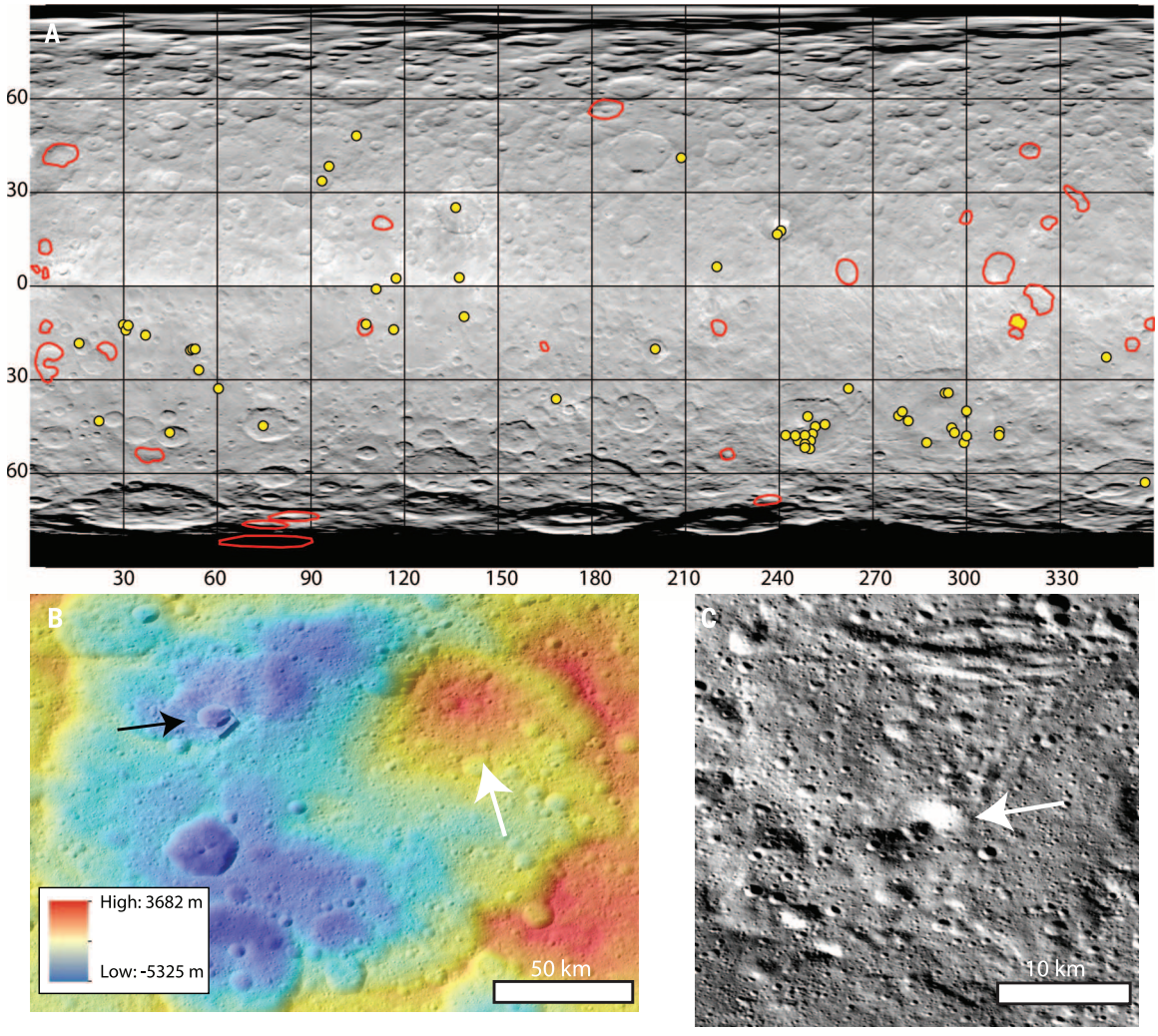

Fig. 7. Domical features on Ceres. (**A**) Global map, based on HAMO (140 m/pixel) grayscale imagery. Large domes are outlined in red; small mounds are marked by yellow dots. Ahuna Mons is the red outline filled in with yellow. (**B**) Color HAMO topography model over HAMO grayscale image of a 53-km dome at 42°N, 10°E, located within an unnamed 135-km crater. The white arrow points to the large dome; the black arrow points to nearby Oxo crater, where surface water ice has been identified (*47*). (**C**) LAMO (35 m/pixel) grayscale image of small mound (white arrow) with a summit pit identified in Yalode crater at 45.5°S, 295.7° E.

near the Samhain Catenae (Fig. 6E), which are consistent with models of asymmetrical domal uplift (*31*). This system shows apparent broad outer arc extension, with at least two central peaks (Fig. 6E, black arrows). Away from these peaks, the fracturing transitions to radial fault patterns, which geological models have shown can occur due to the change in stress orientation that occurs at the edge of a dome (*31*).

Similar structures form on the surface of salt domes on Earth (*31*). Terrestrial salt domes form when layers of evaporite minerals are buried under a denser overburden material; salts are buoyant under these conditions and can intrude into the overlying rock strata (*32*). Differential loading of the overburden material is a driving force in terrestrial salt tectonics, but thick layers of either the cover material or the salt itself are not necessarily required (*33*). Instead, salt flow can occur where there is a laterally varying (*32*), or even a thin (*33*), overburden thickness. The growth of the salt diapirs then creates pressure on the surface materials, deforming the overlying material. Where the salt extrudes onto the surface, lobate flows can form.

Salt tectonics is at least theoretically possible on Ceres. Layers of salt have long been hypothesized to exist deep within the so-called ocean worlds (*34*–*37*), which include Ceres (*34*). Compositional upwelling similar to terrestrial salt dome formation has even been hypothesized to occur (*35*). The interior of Ceres has been determined to contain a silicate core, a water-rich mantle, and a mechanically strong crust (*3*). The main components of the crust were determined to be rock, ice, and salt hydrates (*3*), including carbonates (*38*), ammoniated phyllosilicates (*38*, *39*), and a dark material that is thought to be magnetite (*38*). Although these crustal materials are not particularly dense, the putative subsurface salts would have even lower densities (*28*), and so salt diapirism could potentially occur. The structure patterns identified on the surface of Ceres (Fig. 6E), while not exclusively indicative of salt upwelling, are certainly suggestive of it.

Domes and mounds

Domical features on Ceres fall into two broad classes: large domes that are 10s to 100s of kilometers in diameter, with heights 1 to 5 km, and small mounds <10 km in diameter exhibiting subkilometer relief (Fig. 7). However, whether or not a single formation mechanism is responsible for their formation is still an open question. The 28 large domes identified in HAMO images are circular to ovoid in plan form, are 30 to 100 km in diameter, and typically exhibit 2 to 5 km of relief (Fig. 7B). They are commonly, but not exclusively, located in large impact basins. Detailed geomorphic analysis and physical modeling of the 4-km-high Ahuna Mons suggest that this large dome is most likely a cryovolcanic edifice formed by the extrusion of a viscous water-ice-silicate mixture (*19*). The other large domical features (Fig. 7A, red outlines) are suggested to also be cryovolcanic in nature, although perhaps of a different age and/or rheology (*19*).

Of the ~200 small mounds identified (Fig. 7A, yellow dots), many are located preferentially in smooth regions associated with impact materials. These mounds are thus most likely impact debris, or possibly preexisting topography embayed or draped by smooth material, analogous to mounds observed in lunar-impact melt sheets. Early analysis of these features was motivated by the expectation that localized cryovolcanic activity or frost-heave phenomena might occur in crater interiors soon after impact if Ceres' shallow subsurface were ice-rich. So far there is little morphological evidence that these features are genetically related to ice, although there are individual small

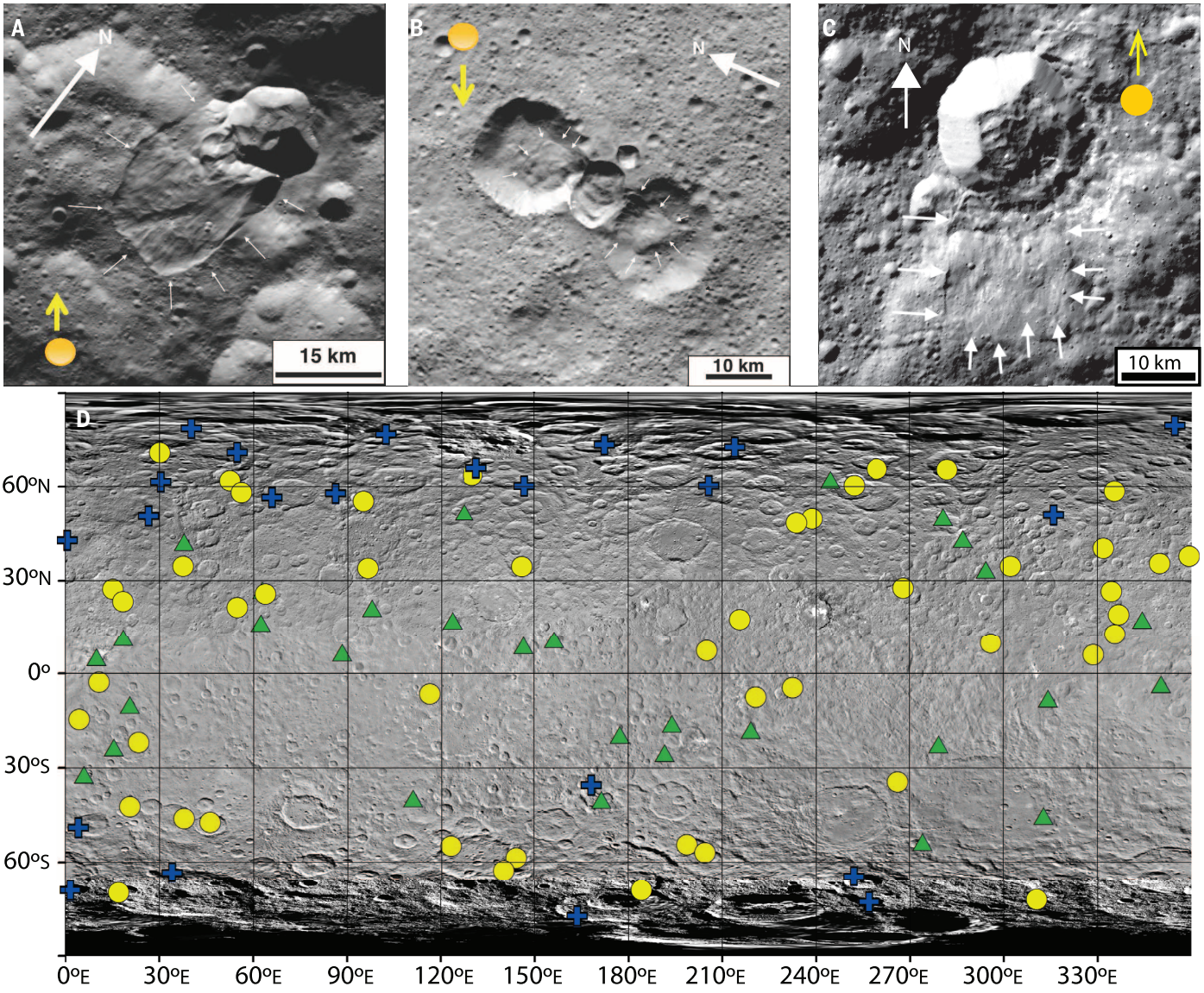

Fig. 8. Lobate flows on Ceres. White arrows point to flow margins. Yellow arrows point away from the Sun (yellow dot) in the direction of illumination. (**A**) Type 1 flow. (**B**) Type 2 flow. (**C**) Type 3 flow. (**D**) Location of lobate flows on Ceres. Blue crosses represent Type 1 flows, green triangles are Type 2 flows, and yellow dots are Type 3 flows.

mounds (e.g., Fig. 7C) for which an ice-rich origin cannot be ruled out.

Lobate flows

A range of mass-wasting flows are observed across the surface of Ceres, and differences in their morphology suggest that multiple emplacement processes might be operative. These features, which are always associated, either internally or externally, with the rims of impact craters, are broadly divided into three types, based on their morphology.

Type 1 flows (Fig. 8A) are lobate, have notably steep frontal toes, and are usually >100 m thick at their termini. They are as wide as their source, possessing nested sets of parallel linear furrows 10s of meters deep along the direction of downslope motion and steep-fronted toes with distal ramparts. These lobate flows occur in high-latitude craters and morphologically are similar to ice-cored and ice-cemented flows on Earth (*40*, *41*) and Mars (*42*). Type 1 flows are found typically above 50° latitude (Fig. 8D).

Type 2 flows (Fig. 8B) have long, fan-shaped thin flows that originate at a crater wall. Thinner than Type 1 flows (generally between 10 and 100 m thick at their termini), they traverse generally longer distances despite their shallow slopes. They range from relatively narrow to broad, having conical to lobate shapes, but are always composed of platy sheets with rounded tapered toes. Morphologically, these flows are similar to long-runout landslides found on icy satellites such as Iapetus (*43*). Type 2 flows are found across Ceres but mainly at mid to high latitudes (Fig. 8D).

In Type 3 flows (Fig. 8C), broad sheets of smooth material, which are thinner than Type 1 flows at 10 to 100 m thick at their termini, extend outward from crater rims, terminating in layered sets of lobes or cusps. Their acute triangular lobes, absence of deep furrows, and textures—relatively smooth surfaces interspersed with hummocky regions—are similar to the morphology of fluidized ejecta blankets of rampart craters on Mars [e.g., (*44*, *45*)] and Ganymede (*46*), features that are commonly thought to form by impact into ice-rich ground. Type 3 flows are found in low to mid latitudes (Fig. 8D) and are wider than Type 2 flows.

Discussion and conclusions

The lack of a large inventory of relaxed craters on Ceres suggests that its crust is too strong to be dominated by ice (*3*, *6*, *7*). Similarly, the presence of ancient surface fractures, and extensive subsurface fracturing (as demonstrated by the widespread distribution of polygonal craters), is more consistent with a mechanically strong crust, not

an ice-dominated crust (*3*). These observations are consistent with spectroscopic analyses that have currently identified surface water ice at only one location on Ceres (*47*). However, studies have shown that a crust strong enough for both negligible crater relaxation and the preservation of linear structures could be provided by a mixture of ice, rock, and/or salt hydrates (*48*).

The identification of potentially ice-related geomorphic features suggests that there may be some ice in localized regions in the crust on Ceres. Global mapping of the lobate flows shows that there is a latitudinal trend in the distribution of the observed type morphologies (Fig. 8D). This, along with their morphologic similarity to features that form on other planetary bodies by varying ice-related processes, suggests that the differences in lobate flow morphology might be explained by variations in ice content and temperature in the near surface.

Likewise, there is geomorphic evidence that the interior of Ceres is ice-rich, as models (*3*) have suggested. Geomorphic and topographic analyses of the FFCs suggest that cryomagmatism has been active on Ceres. The central dome on the floor of Occator crater also indicates that cryomagmatism may have occurred. In addition, Ahuna Mons and the other large domes appear to be cryovolcanic in nature (*19*).

In conclusion, although the observed geomorphic features are not consistent with an ice-dominated crust, they are consistent with Ceres having an ice-rich upper mantle and a crust that is composed of a rock-ice mixture.

REFERENCES AND NOTES

1. C. T. Russell, C. A. Raymond, The Dawn mission to Vesta and Ceres. *Space Sci. Rev.* **163**, 3–23 (2011). doi: 10.1007/s11214-011-9836-2
2. H. Sierks *et al*., The Dawn Framing Camera. *Space Sci. Rev.* **163**, 263–327 (2011). doi: 10.1007/s11214-011-9745-4
3. C. T. Russell *et al*., Dawn arrives at Ceres: Exploration of a small, volatile-rich world. *Science* **353**, 1008–1010 (2016).
4. R. A. Yingst *et al*., Geologic mapping of Vesta. *Planet. Space Sci.* **103**, 2–23 (2014). doi: 10.1016/j.pss.2013.12.014
5. R. Jaumann *et al*., Vesta's shape and morphology. *Science* **336**, 687–690 (2012). doi: 10.1126/science.1219122; pmid: 22582254
6. H. Hiesinger *et al*., Cratering on Ceres: Implications for its crust and evolution. *Science* **353**, aaf4759 (2016).
7. M. T. Bland, Predicted crater morphologies on Ceres: Probing internal structure and evolution. *Icarus* **226**, 510–521 (2013). doi: 10.1016/j.icarus.2013.05.037
8. R. D. Lorenz *et al*., Hypsometry of Titan. *Icarus* **211**, 699–706 (2011). doi: 10.1016/j.icarus.2010.10.002
9. M. Küppers *et al*., Localized sources of water vapour on the dwarf planet (1) Ceres. *Nature* **505**, 525–527 (2014). doi: 10.1038/nature12918; pmid: 24451541
10. A. Nathues *et al*., Sublimation in bright spots on (1) Ceres. *Nature* **528**, 237–240 (2015). doi: 10.1038/nature15754; pmid: 26659183
11. P. M. Schenk, Central pit and dome craters: Exposing the interiors of Ganymede and Callisto. *J. Geophys. Res.* **98** (E4), 7475–7498 (1993). doi: 10.1029/93JE00176
12. V. J. Bray, P. M. Schenk, H. J. Melosh, J. V. Morgan, G. S. Collins, Ganymede crater dimensions – Implications for central peak and central pit formation and development. *Icarus* **217**, 115–129 (2012). doi: 10.1016/j.icarus.2011.10.004
13. P. H. Schultz, Floor-fractured lunar craters. *Moon* **15**, 241–273 (1976). doi: 10.1007/BF00562240
14. L. M. Jozwiak, J. W. Head, M. T. Zuber, D. E. Smith, G. A. Neumann, Lunar floor-fractured craters: Classification, distribution, origin and implications for magmatism and shallow crustal structure. *J. Geophys. Res.* **117**, 2012JE004134 (2012). doi: 10.1029/2012JE004134
15. L. M. Jozwiak, J. W. Head, L. Wilson, Lunar floor-fractured craters as magmatic intrusions: Geometry, modes of emplacement, associated tectonic and volcanic features, and implications for gravity anomalies. *Icarus* **248**, 424–447 (2015). doi: 10.1016/j.icarus.2014.10.052
16. J. L. Hall, S. C. Solomon, J. W. Head, Lunar floor-fractured craters: Evidence of viscous relaxation of crater topography. *J. Geophys. Res.* **86** (B10), 9537–9552 (1981). doi: 10.1029/JB086iB10p09537
17. M. Bamberg, R. Jaumann, H. Asche, T. Kneissl, G. G. Michael, Floor-fractured craters on Mars – Observation and origin. *Planet. Space Sci.* **98**, 146–162 (2014). doi: 10.1016/j.pss.2013.09.017
18. A. J. Dombard, J. Gillis, Testing the viability of topographic relaxation as a mechanism for the formation of lunar floor-fractured craters. *J. Geophys. Res.* **106** (E11), 27901–27909 (2001). doi: 10.1029/2000JE001388
19. O. Ruesch *et al*., Cryovolcanism on Ceres. *Science* **353**, aaf4286 (2016).
20. P. C. Thomas *et al*., Mathilde: Size, shape and geology. *Icarus* **140**, 17–27 (1999). doi: 10.1006/icar.1999.6121
21. L. Prockter *et al*., Surface expressions of structural features on Eros. *Icarus* **155**, 75–93 (2002). doi: 10.1006/icar.2001.6770
22. M. Massironi *et al*., Geological map and stratigraphy of asteroid 21 Lutetia. *Planet. Space Sci.* **66**, 125–136 (2012). doi: 10.1016/j.pss.2011.12.024
23. C. C. Porco *et al*., Cassini imaging science: Initial results on Phoebe and Iapetus. *Science* **307**, 1237–1242 (2005). doi: 10.1126/science.1107981; pmid: 15731440
24. C. B. Beddingfield, D. M. Burr, L. T. Tran, Polygonal impact craters on Dione: Evidence for tectonic structures outside the wispy terrain. *Icarus* **274**, 163–194 (2016). doi: 10.1016/j.icarus.2016.03.020
25. D. T. Eppler, R. Ehrlich, D. Nummedal, P. H. Schultz, Sources of shape variation in lunar impact craters – Fourier shape analysis. *Geol. Soc. Am. Bull.* **94**, 274–291 (1983). doi: 10.1130/0016-7606(1983)94<274:SOSVIL>2.0.CO;2
26. T. Öhman, M. Aittola, V.-P. Kostama, J. Raitala, J. Korteniemi, Polygonal impact craters in Argyre region Mars: Implications for geology and cratering mechanics. *Meteorit. Planet. Sci.* **43**, 1605–1628 (2008). doi: 10.1111/j.1945-5100.2008.tb00632.x
27. V. R. Oberbeck, R. H. Morrison, Laboratory simulation of the herringbone pattern associated with lunar secondary crater chains. *Moon* **9**, 415–455 (1974). doi: 10.1007/BF00562581
28. D. L. Buczkowski, D. Y. Wyrick, Tectonism and magmatism identified on asteroids. *Geol. Soc. Lond. Spec. Publ.* **401**, 423–441 (2014). doi: 10.1144/SP401.18
29. D. Y. Wyrick, D. A. Ferrill, A. P. Morris, S. L. Colton, D. W. Sims, Distribution, morphology, and origins of martian pit crater chains. *J. Geophys. Res.* **109**, E06005 (2004). doi: 10.1029/2004JE002240
30. D. L. Buczkowski, O. S. Barnouin-Jha, L. M. Prockter, 433 Eros lineaments: Global mapping and analysis. *Icarus* **193**, 39–52 (2008). doi: 10.1016/j.icarus.2007.06.028
31. D. W. Sims *et al*., Analog modeling of normal faulting above Middle East domes during regional extension. *Am. Assoc. Pet. Geol. Bull.* **97**, 877–898 (2013).
32. M. R. Hudec, M. P. A. Jackson, Terra infirma: Understanding salt tectonics. *Earth Sci. Rev.* **82**, 1–28 (2007). doi: 10.1016/j.earscirev.2007.01.001
33. J.-P. Brun, X. Fort, Salt tectonics and passive margins: Geology versus models. *Mar. Pet. Geol.* **28**, 1123–1145 (2011). doi: 10.1016/j.marpetgeo.2011.03.004
34. J. C. Castillo-Rogez, T. B. McCord, Ceres' evolution and present state constrained by shape data. *Icarus* **205**, 443–459 (2010). doi: 10.1016/j.icarus.2009.04.008
35. J. S. Kargel *et al*., Europa's crust and ocean: Origin, composition and the prospects for life. *Icarus* **148**, 226–265 (2000). doi: 10.1006/icar.2000.6471
36. N. A. Spaun, J. W. Head III, A model of Europa's crustal structure: Recent Galileo results and implications for an ocean. *J. Geophys. Res.* **106** (E4), 7567–7576 (2001). doi: 10.1029/2000JE001270
37. M. Y. Zolotov, An oceanic composition on early and today's Enceladus. *Geophys. Res. Lett.* **34**, 2007GL031234 (2007). doi: 10.1029/2007GL031234
38. M. C. De Sanctis *et al*., Ammoniated phyllosilicates with a likely outer solar system origin on (1) Ceres. *Nature* **528**, 241–244 (2015). doi: 10.1038/nature16172; pmid: 26659184
39. E. Ammannito *et al*., Distribution of phyllosilicates on Ceres. *Science* **353**, aaf4279 (2016).
40. S. E. White, Rock glaciers and block fields, review and new data. *Quat. Res.* **6**, 77–97 (1976). doi: 10.1016/0033-5894(76)90041-7
41. O. Humlum, The geomorphic significance of rock glaciers: Estimates of rock glacier debris volumes and headwall recession rates in West Greenland. *Geomorphology* **35**, 41–67 (2000). doi: 10.1016/S0169-555X(00)00022-2
42. J. W. Holt *et al*., Radar sounding evidence for buried glaciers in the southern mid-latitudes of Mars. *Science* **322**, 1235–1238 (2008). doi: 10.1126/science.1164246; pmid: 19023078
43. K. N. Singer, W. B. McKinnon, P. M. Schenk, J. M. Moore, Massive ice avalanches on Iapetus mobilized by friction reduction during flash heating. *Nat. Geosci.* **5**, 574–578 (2012). doi: 10.1038/ngeo1526
44. M. H. Carr *et al*., Martian impact craters and emplacement of ejecta by surface flow. *J. Geophys. Res.* **82**, 4055–4065 (1977). doi: 10.1029/JS082i028p04055
45. L. E. Senft, S. T. Stewart, Impact crater formation into icy layered terrains on Mars. *Met. Planet. Sci.* **43**, 1993–2013 (2008). doi: 10.1111/j.1945-5100.2008.tb00657.x
46. J. Boyce, N. Barlow, P. Mouginis-Mark, S. Stewart, Rampart craters on Ganymede: Their implications for fluidized ejecta emplacement. *Met. Planet. Sci.* **45**, 638–661 (2010). doi: 10.1111/j.1945-5100.2010.01044.x
47. J.-Ph. Combe *et al*., Detection of local H_2O exposed at the surface of Ceres. *Science* **353**, aaf3010 (2016).
48. W. B. Durham, S. H. Kirby, L. A. Stern, Effects of dispersed particulates on the rheology of water ice at planetary conditions. *J. Geophys. Res.* **97**, 20883–20897 (1992). doi: 10.1029/92JE02326

ACKNOWLEDGMENTS

We thank the Dawn Operations team, the Flight team, and the Instrument teams for all their work. M.B. and N.S. thank NASA's Dawn at Ceres Guest Investigator Program for support. Dawn data are archived with the NASA Planetary Data System. (http://pds-smallbodies.astro.umd.edu/data_sb/missions/dawn/index.shtml). D.L.B. wrote the manuscript and coordinated coauthor contributions; performed the analysis of linear structures, Occator structures, and FFCs; and participated in the geologic mapping. B.E.S. led the Ground Ice Working group and the analysis of lobate flows. D.A.W., S.C.M., and J.E.C.S. participated in the Survey global geologic map. A.I.E. evaluated the Ceres hypsogram, and F.P. worked on the Ceres topography. P.S., K.A.O., H.H., D.O., S.M., and T.P. all contributed to the evaluation of Ceres craters. P.S. led the study of Occator's central dome and its similarity to central domes on other icy bodies. H.S. mapped the global extent of domes, and K.H. mapped the global extent of lobate flows. H.C., S.B., M.B., H.S., and T.P. participated in the evaluation of potential ice-cored features. R.J., T.R., M.V.S., A.N., M.C.D.S., and C.A.R. provided useful comments and suggestions during manuscript preparation. C.T.R. is the mission principal investigator and guided the research.

SUPPLEMENTARY MATERIALS

www.sciencemag.org/content/353/6303/aaf4332/suppl/DC1
Figs. S1 to S3

6 February 2016; accepted 22 July 2016
10.1126/science.aaf4332

The geomorphology of Ceres

D. L. Buczkowski, B. E. Schmidt, D. A. Williams, S. C. Mest, J. E. C. Scully, A. I. Ermakov, F. Preusker, P. Schenk, K. A. Otto, H. Hiesinger, D. O'Brien, S. Marchi, H. Sizemore, K. Hughson, H. Chilton, M. Bland, S. Byrne, N. Schorghofer, T. Platz, R. Jaumann, T. Roatsch, M. V. Sykes, A. Nathues, M. C. De Sanctis, C. A. Raymond and C. T. Russell

Science **353** (6303), aaf4332.
DOI: 10.1126/science.aaf4332